PROCEEDINGS OF SCIENCE

Deconfinement in neutron stars by Color-Spin-Molecular-Dynamics

Nobutoshi Yasutake[a,b,*] **and Toshiki Maruyama**[b]

[a] *Department of Physics, Chiba Institute of Technology, 2-1-1 Shibazono, Narashino, Chiba, 275-0023, Japan*

[b] *Advanced Science Research Center, Japan Atomic Energy Agency, Tokai, Ibaraki, 319-1195, Japan*

E-mail: nobutoshi.yasutake@p.chibakoudai.jp, maruyama.toshiki@jaea.go.jp

We focus on the equation of state in neutron stars with the color-spin molecular dynamics. This is based on the constituent quark model, and reproduces the quark confinement/deconfinement phenomena by solving the degrees of freedom of color and spin for each quark. The equation of state for dense matter is studied, and it replicates the saturation properties: symmetric energy, L-parameter, and incompressibility around nuclear density. The resultant mass-radius relations are consistent with the observations such as the gravitational wave observations, NICER etc. Our numerical results suggest that de-confined quark matter appears in the core of neutron stars via crossover. Although the current constraints from the observations are not enough to conclude whether quark matter appears at high-density region, our method would help to understand high-density material properties inside neutron stars in the future.

The XVIth Quark Confinement and the Hadron Spectrum Conference (QCHSC24)
19-24 August, 2024
Cairns Convention Centre, Cairns, Queensland, Australia

*Speaker

© Copyright owned by the author(s) under the terms of the Creative Commons Attribution-NonCommercial-NoDerivatives 4.0 International License (CC BY-NC-ND 4.0) All rights for text and data mining, AI training, and similar technologies for commercial purposes, are reserved. ISSN 1824-8039 . Published by SISSA Medialab.

PoS(QCHSC24)221

1. Introduction

Understanding the internal states of neutron stars through astrophysical observations, such as those from the Neutron Star Interior Composition Explorer (NICER) [1–4] and gravitational wave detectors [5], has become a prominent research focus in recent years. Instead of solely analyzing individual celestial objects or phenomena to constrain the equation of state (EOS) for high-density matter, recent trends emphasize comprehensively interpreting observational results using statistical methods, including machine learning approaches.

Regarding densities near saturation, several constraints have been extensively derived over the past quarter-century through various nuclear experiments and theoretical models, including heavy-ion collision experiments. The binding energy per baryon S_0 for symmetric nuclear matter has conventionally been known to be approximately -16 MeV. Additionally, the symmetry energy J, which represents the energy difference per baryon between symmetric nuclear matter and pure neutron matter, is also constrained within a relatively narrow range, as 29-33 MeV [6, 7]. However, the values of the slope of the energy for neutron matter known as "L-parameter", and the incompressibility for symmetric matter K_0 are highly model-dependent.

In this study, the incompressibility K_0 is assumed to be around 250 MeV. This value lies within the constraints proposed by Danielewicz et al., who analyzed matter flow to extract pressures in nuclear collisions, suggesting $167 < K_0 < 300$ MeV [8]. It is also consistent with Piekarewicz's result of $K_0 = 248 \pm 8$ MeV, derived from the iso-scalar giant monopole resonance (ISGMR) in ^{208} Pb using the relativistic mean-field model with a random-phase approximation [9]. However, it should be noted that these values are not definitive, as some studies suggest smaller values. For example, Sturm et al. and Hartnack et al. concluded that K_0 is approximately 200 MeV based on transport theory applied to experimental data from heavy-ion collisions [10, 11]. Additionally, the analysis of ISGMR measurements in medium-heavy nuclei by G. Col et al., who used various Skyrme forces, predicts K_0 around 230 MeV [12].

For L-parameters, the ratio of uncertainty to their values is even larger than that for incompressibility K_0. Nevertheless, these parameters play a critical role in determining the equation of state (EOS) and material structure. It is well known that L-parameters are key factors in shaping the structure of pasta phases near subnuclear densities. In this study, we adopt a fiducial range for the L-parameter of $L = 60 \pm 20$ MeV, based on constraints derived from analyses of terrestrial experiments, as summarized in Refs.[7, 13].

In this study, building on previous research, we aim to determine an equation of state for high-density matter that satisfies these constraints using our Color-Spin Molecular Dynamics (CSMD) calculations.

2. Formulation

Here, we outline the formulation of the CSMD calculations, which is extended from our previous researches focused on the time evolution of the color degrees of freedom through Color-Molecular Dynamics (CMD) calculations [14–16]. Adding the color degrees of freedom, the aim

PoS(QCHSC24)221

of this study is to solve the spin evolution [1]. In this study, the total wave function for N-quark system is expressed as the direct products of single-quark packets, characterized by their positions, momenta, and internal degrees of freedom as follows:

$$\Psi(\mathbf{r}_1, \mathbf{r}_2, ...\mathbf{r}_N) = \prod_{i=1}^{N} \frac{1}{(\pi {L_q}^2)^{3/4}} \exp\left[-\frac{(\mathbf{r}_i - \mathbf{R}_i)^2}{2{L_q}^2} + \frac{i}{\hbar}\mathbf{P}_i\mathbf{r}_i\right]\chi_i, \tag{1}$$

where $\mathbf{r_i}$ represents the coordinates of the i-th particle within the Gaussian wave packet centered at $\mathbf{R}_i$, while $\mathbf{P}_i$ denotes the momentum at the center of each wave packet, and χ_i represents the internal degree of freedom. The parameter L_q is introduced to define the width of the wave packets and is set as $L_q = 0.33$ fm in this work.

The internal degree of freedom χ_i is expressed as the direct product of the flavor component χ_i^f, the color component χ_i^c, and the spin component χ_i^s as $\chi_i = {\chi_i}^f {\chi_i}^c {\chi_i}^s$. The explicit form of the time-dependent degree of freedom for color is shown as

$${\chi_i}^c = \begin{pmatrix} \cos\alpha_i \; e^{-i\beta_i} \; \cos\theta_i \\ \sin\alpha_i \; e^{i\beta_i} \; \cos\theta_i \\ \sin\theta_i \; e^{i\varphi_i} \end{pmatrix}, \quad \chi_i^S = \begin{pmatrix} e^{-i\beta_i^S} \cos\alpha_i^S \\ e^{i\beta_i^S} \sin\alpha_i^S \end{pmatrix}, \tag{2}$$

where $\alpha_i, \beta_i, \theta_i, \varphi_i$ are the degrees of freedom related with colors, while α_i^S, β_i^S are for the degrees of freedom related of $i-$th particle. Regarding flavors, they are fixed for the calculations of the energy for neutron matter and symmetric matter. However, when obtaining the beta equilibrium and the charge neutrality conditions, which are realized inside neutron stars, the flavor conversion process is performed via $u + e \leftrightarrow d$. Energy calculations incorporate electrons to determine the most stable state and reproduce these conditions. Furthermore, by employing the large-N limit approximation, the spin degrees of freedom are allowed to evolve over time within this framework, ultimately yielding the most stable states for both color and spin.

This system follows the Hamiltonian described below.

$$H = \left\langle \Psi \left| \sum_{i=1}^{N} \sqrt{m + \hat{\mathbf{p}}_i^2} + \hat{V}_{\rm C} + \hat{V}_{\rm M} + \hat{V}_{\rm CM} \right| \Psi \right\rangle. \tag{3}$$

The first term corresponds to the relativistic kinetic energy, followed by terms representing the color-related interactions, the quark-meson interactions, and the interactions associated with both color and spin, known as the color-magnetic interaction. In our model, the gluon and meson degrees

[1] In our calculations here, we essentially employ the same method that was introduced in Ref. [17]. However, we have further developed that method by introducing a spin friction term with the coefficient μ_S, which works according to the time evolution of the spin:

$$\dot{\alpha_i^S} = \frac{1}{2\hbar \sin 2\alpha_i^S}\frac{\partial H}{\partial \beta_i^S} - \mu_S \frac{\partial H}{\partial \alpha_i^S}$$
$$\dot{\beta_i^S} = -\frac{1}{2\hbar \sin 2\alpha_i^S}\frac{\partial H}{\partial \alpha_i^S} - \mu_S \frac{\partial H}{\partial \beta_i^S},$$

where μ_S is set to 0.1. As a result, the optimization of the spin is facilitated, allowing the system's energy to converge more rapidly to the most stable configuration—this represents an advancement in our approach.

PoS(QCHSC24)221

of freedom are not explicitly resolved; instead, their effects are incorporated into the interactions between quarks.

The second term is consist with the confinement term (the first term) and the one gluon exchange term (the second term) expressed as

$$\hat{V}_C = -\frac{1}{2}\sum_{i.j\neq i}^{N}\sum_{a=1}^{8}\frac{\lambda_i^a\lambda_j^a}{4}\left(\kappa\hat{r}_{ij} - \frac{\alpha_s}{\hat{r}_{ij}}\right), \tag{4}$$

where $\hat{r}_{ij}$ represents the distance between quarks i and j, while λ_i^a denotes the Gell-Mann matrix for color. The initial factor of 1/2 is included to avoid double counting of interactions between particle pairs. The coupling constants are set as $\kappa = 0.75$ GeV fm^{-1} and $\alpha_S = 1.25$.

We assume the quark-meson interactions as q-ω, q-σ, and q-ρ couplings, expressed as follows:

$$\hat{V}_{\rm M} = \frac{1}{2}\sum_{i}^{N}\left[\frac{g_\omega^2 C_\omega}{4\pi}\left(\sum_{j\neq i}^{N}\frac{e^{-\mu_\omega r_{ij}}}{r_{ij}}\right)^{1+\epsilon_\omega} - \frac{g_\sigma^2 C_\sigma}{4\pi}\left(\sum_{j\neq i}^{N}\frac{e^{-\mu_\sigma r_{ij}}}{r_{ij}}\right)^{1+\epsilon_\sigma} + \sum_{j\neq i}^{N}\frac{\tau_i^3\tau_j^3}{4}\frac{g_\rho^2}{4\pi}\frac{e^{-\mu_\rho r_{ij}}}{r_{ij}}\right], \tag{5}$$

where the coupling constant are set as g_ω=5.60, g_σ=3.41, g_ρ=4.09, while the meson masses μ_ω, μ_σ, and μ_ρ are set as $\mu_\omega = 782.6$ MeV, $\mu_\sigma = 400$ MeV, and $\mu_\rho = 770$ MeV, respectively. Regarding q-ω, q-σ interactions, we assume the non-linearity introducing ϵ_ω and ϵ_σ. Without them, these interactions works only between i and j particles, representing two-body correlations. Therefore, the physical interpretation of this nonlinearity reflects many-body interactions. This implies that the quark-meson couplings not only account for pairwise interactions but also include the collective effects arising from the dense medium. Such nonlinearity naturally emerges in systems where the interplay between quarks and mesons introduces higher-order terms or effective potentials, representing correlations and screening effects among multiple particles. These many-body effects are crucial for accurately describing EOSs in dense matter, such as neutron star interiors, and for understanding the emergence of collective phenomena like clustering or phase transitions. In this work, we set as ϵ_ω=0.15, and $\epsilon_\sigma = -0.21$. Related with these parameters, we also introduce C_ω, C_σ, which are defined to make the coupling constants dimensionless, set as $C_\omega = 1/(1+\epsilon_\omega)$, $C_\sigma = 1/(1+\epsilon_\sigma)$ [15, 16].

As we described, we have extended our calculations to include not only the color degree of freedom but also the time evolution of the spin degree of freedom in this work. The interaction involving both of these degrees of freedom is the color-magnetic interaction, which is expressed as follows:

$$\hat{V}_{\rm CM} = \frac{1}{2}\sum_{i.j\neq i}^{N}\sum_{a=1}^{8}\sum_{b=1}^{3}\frac{g_{\rm CS}}{m_i m_j r_{0ij}^2}\frac{\exp(-(r_{ij}/r_{0ij})^2)}{r_{ij}}\frac{\lambda_i^a\lambda_j^a}{4}\frac{\sigma_i^b\sigma_j^b}{4}, \tag{6}$$

where r_{0ij} represents the effective range of the interaction, defined as $r_{0ij} = 1/(\alpha+\beta\mu_{ij})$, where $\mu_{ij} = m_i m_j/(m_i+m_j)$ is the reduced mass. The coupling constant for the color-spin interaction, $g_{\rm CS}$, is set to $g_{\rm CS} = 1.34$. The parameters α and β, which determine the effective range dependence on the reduced mass, are chosen as $\alpha = 2.1$ fm^{-1} and $\beta = 0.552$, as provided in Ref. [18]. This term represents the intricate interplay between spin and color degrees of freedom, which is a distinctive feature of Quantum Chromodynamics (QCD). Its inclusion is essential for capturing the dynamics

PoS(QCHSC24)221

of quarks in dense matter, as it governs phenomena such as the alignment of spins and color states, ultimately influencing the macroscopic properties of the system.

In this study, calculations were performed for an infinite system by imposing periodic boundary conditions. Consequently, approximations based on the large-N limit were employed for the spin and color degrees of freedom.That is, the spin correlation is expressed as follows:

$$\begin{aligned} <\uparrow\uparrow>=<\downarrow\downarrow>= \frac{1}{4}, \\ <\uparrow\downarrow>= -\frac{1}{4}, \end{aligned} \tag{7}$$

where the meaning of the notation is defined as

$$<\uparrow\uparrow>\equiv<\uparrow\uparrow |\sigma_a\sigma_a| \uparrow\uparrow> . \tag{8}$$

Similarly, the color correlation is given by:

$$\begin{aligned} < RR >=< GG >=< BB >= \frac{4}{3}, \\ < RG >=< GB >=< BR >= -\frac{2}{3}, \end{aligned} \tag{9}$$

where the meaning of the notation is defined as

$$< RR >\equiv< RR|\lambda_a^c\lambda_a^c|RR > . \tag{10}$$

3. Results

The results based on the aforementioned formulation are presented below. In Figure 1, we show the energy per baryon for various systems: ud-matter, udd-matter, and the results for charge-neutral and beta-equilibrated matter, where electrons are included. Note that we cannot simply equate ud-matter and udd-matter to symmetric nuclear matter and neutron matter, respectively, even when quarks are confined at low density. As a result of spin evolution, individual spins do not simply align up or down, indicating that they do not strictly form neutrons or protons. We will revisit this point for further discussion later, but this is due to the large N-system approximation shown in Eq. (7). For reference, we also include in this figure the results for ud-matter and udd-matter, where the spin degrees of freedom are fixed: ud-matter corresponds to symmetric nuclear matter, and udd-matter corresponds to neutron matter in this case. It can be observed that when the spin degree of freedom is allowed to evolve, the optimization results in a slightly lower energy.

As we will see later, the spin configuration resulting from spin evolution differs from that of neutrons and protons. Consequently, a direct comparison with experimental nuclear physics results is not straightforward. However, for reference, Table 1 presents various parameters near the saturation density obtained from ud-matter and udd-matter. These parameters correspond to the coefficients at each order by performing a Taylor expansion around the saturation density n_0. Following convention, the variables are nondimensionalized by $3n_0$, and the coefficients at each order are listed except for the factorial in the denominator. From the zeroth order, the coefficients are represented by the letters S, L, and K, with a subscript “0" attached for ud-matter. For the

PoS(QCHSC24)221

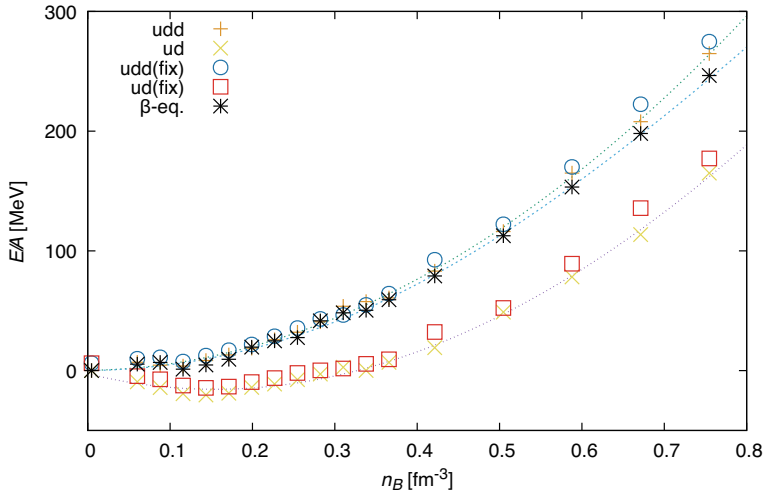

Figure 1: Density dependence of energy per baryon E/A for each matter ud-matter and udd-matter with spin-evolutions. The data points, labeled by "β-eq.", are obtained E/A under the charge-neutral and beta-equilibrium conditions added the contribution of electrons. Here, we present the calculation results for two cases: one with fixed spin (labeled as "fix") and one where the spin degrees of freedom are allowed to evolve. Each data point represents the numerical results. Thin dot lines are the regression curves of them.

zeroth-order coefficient, instead of listing the coefficient for udd-matter, we follow convention by presenting the difference from ud-matter, denoted as $J(= S - S_0)$. All values are consistent with the results of previous nuclear experiments introduced in the introduction. Regarding K, we do not reflect any experimental results. In the future, once a definitive constraint on K is obtained, we will reconsider its inclusion. At present, nuclear experiments can at most constrain up to the second order. To determine higher-order terms, we must rely on astronomical observations.

Figure 2 illustrates the mass-radius (MR) relation of NSs derived from the equation of state presented in Figure 1. For densities below the subnuclear density $n_B < 0.06$ fm^{-3}, we adopt the EOS formulated by Baym, Pethick, and Sutherland [19]. We also include constraints from several representative MR diagrams based on astronomical observations: the constraints with NICER from PSR J0030+0451 [1, 2], the constraint from MSP J0740+6620 obtained by the NICER and XMM-Newton data sets [3, 4], the gravitational wave observation on GW170817 [5], the expected lower limit of radii of NSs by Bauswein et al. based on the analysis on the electromagnetic (EM) observation accompanied by GW170817 [20], the upper mass limit suggested by numerical relativity [21]. Based on our CSMD results, the maximum mass of a neutron star is 2.23 $M_\odot$, and the tidal deformability is $\Lambda_{1.4\,M_\odot} = 599$, both of which satisfy observational constraints.

Figure 3 illustrates the initial and final configurations in our CSMD calculations for four times

Table 1: Fitting parameters for Figure 1, which corresponds to the coefficients at each order by performing a Taylor expansion around the saturation density n_0 except for the factorial in the denominator. Each physical meaning is shown in the text.

n_0 [fm^{-3}]	S_0 [MeV]	K_0 [MeV]	J [MeV]	L [MeV]
0.154	-15.6	247.3	28.1	71.6

PoS(QCHSC24)221

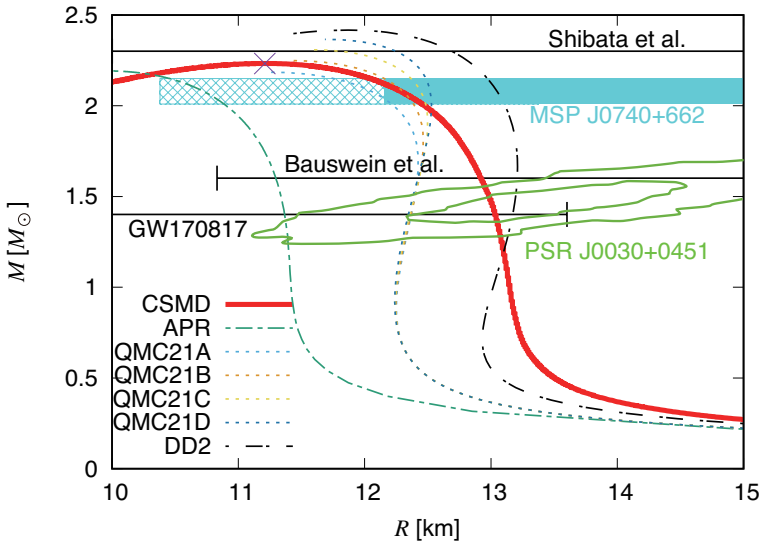

Figure 2: The mass-radius relation obtained from the numerical results of CSMD, where the maximum mass is represented by a cross point. We also show the constraints obtained from the astronomical observations [1–5, 20, 21].

nuclear density, allowed the time evolution of spins. In this figure, the colors have physical meaning: white indicates that quarks are confined in baryons. The bars extending from each particle represent the direction of its spin. In the model where spin degrees of freedom are allowed to evolve, it can be observed that each baryon forms a Y-shaped spin-configuration. Furthermore, each baryon does not exist independently but instead forms clusters. Although not explicitly shown here, an analysis of the number of quarks in each cluster suggests that multiples of three are favored. Although we stated that the white color represents a state in which three quarks are confined, having a different color does not necessarily mean that the quarks are unconfined. For example, when considering a cluster of six quarks that forms a color singlet as a whole, the colors of individual baryons may be

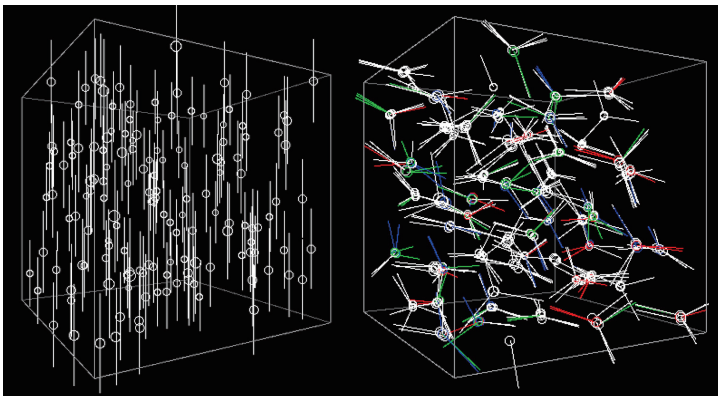

Figure 3: The initial (left) and final (right) configurations at four times of nuclear density are shown. The bars and colors represent the direction of spin and color for particles. White represents a state where three quarks are confined, forming a color singlet baryon.

PoS(QCHSC24)221

entangled between the two baryons. In such cases, if each baryon itself is not color singlet (white), we represent the quarks with their respective colors accordingly. Note that this clustering behavior was not observed before introducing the color-magnetic interaction.

Although the Y-shaped spin configurations and clustering with quark numbers in multiples of three are suggestive, it should be emphasized that these results stem from the large-N approximation (7)(9). While our calculations are conducted in an infinite system with periodic boundary conditions, the results may change if color and spin correlations are determined by the quark numbers within each cluster, where color and spin are strongly entangled, instead of the large-N approximation.

4. Discussion

We have obtained the high-density EOS by repeatedly performing MD calculations that incorporate both color and spin degrees of freedom. For flavor conversion, we directly compute its effects during the calculations by imposing charge neutrality and beta equilibrium. The resulting EOS is consistent with current astronomical observations as well as experimental results such as heavy-ion collisions.

We are extending our calculations to include strangeness now; however, many challenges still remain. Foremost among these is the need to fully relativistically formulate the entire framework—not just the kinetic energy part [22]. Another challenge is how to extend MD calculations to capture condensate phenomena, such as chiral phase transitions and color superconductivity. Of particular interest is determining the number of particles (i.e., the appropriate value of N) to consider when accounting for the combined color and spin degrees of freedom.

We have confirmed that by incorporating the color-magnetic interaction—which had not been included in previous studies—local clustering occurs. However, these configurations are based on the large-N limit approximation. Since our calculations are performed for an infinite system with periodic boundary conditions, we adopted this approximation; nevertheless, the spatial extent of quantum entanglement should be determined by the effective range of the interactions and the regions where clustering occurs.

With the computational framework now established, our future goal is to perform calculations under more realistic physical conditions.

We are grateful to A. Park, S-H. Lee, and T. Hatsuda for fruitful discussions. This work was supported by JSPS KAKENHI Grant Numbers 24K07054. The calculations were performed by the supercomputing system HPE SGI 8600 at the Japan Atomic Energy Agency.

References

[1] T. E. Riley et al., *A NICER View of PSR J0030+0451: Millisecond Pulsar Parameter Estimation*, *Astrophys. J.* **887**, L21 (2019) [astro-ph.HE/1912.05702].

[2] M. C. Miller et al., *PSR J0030+0451 Mass and Radius from NICER Data and Implications for the Properties of Neutron Star Matter*, *Astrophys. J.* **887**, L24 (2019) [astro-ph.HE/1912.05705].

PoS(QCHSC24)221

[3] T. E. Riley et al., *A NICER View of the Massive Pulsar PSR J0740+6620 Informed by Radio Timing and XMM-Newton Spectroscopy*, *Astrophys. J.* **918**, L27 (2021) [astro-ph.HE/2105.06980].

[4] M. C. Miller et al., *The Radius of PSR J0740+6620 from NICER and XMM-Newton Data*, *Astrophys. J.* **918**, L28 (2021) [astro-ph.HE/2105.06979].

[5] B. P. Abbott et al. (The LIGO Scientific Collaboration and the Virgo Collaboration), *GW170817: Observation of Gravitational Waves from a Binary Neutron Star Inspiral*, *Phys. Rev. Lett.* **119**, 161101 (2017) [gr-qc/1710.05832].

[6] M. B. Tsang et al., *Constraints on the symmetry energy and neutron skins from experiments and theory*, *Phys. Rev. C* **86**, 015803 (2012) [nucl-ex/1204.0466].

[7] J. M. Lattimer and Y. Lim, *Constraining the Symmetry Parameters of the Nuclear Interaction*, *Astrophys. J.* **771**, 51 (2013) [nucl-th/1203.4286].

[8] P. Danielewicz, R. Lacey, and W. G. Lynch, *Determination of the Equation of State of Dense Matter*, *Science* **298**, 1592 (2002).

[9] J. Piekarewicz, *Unmasking the nuclear matter equation of state*, *Phys. Rev. C* **69**, 041301 (2004).

[10] C. Sturm et al., *Evidence for a Soft Nuclear Equation-of-State from Kaon Production in Heavy-Ion Collisions*, *Phys. Rev. Lett.* **86**, 39 (2001).

[11] Ch. Hartnack, H. Oeschler, and J. Aichelin, *Hadronic matter is soft*, *Phys. Rev. Lett.* **96**, 012302 (2006) [nucl-th/0506087].

[12] G. Colò, N. Van Giai, J. Meyer, K. Bennaceur, and P. Bonche, *Microscopic determination of the nuclear incompressibility within the nonrelativistic framework*, *Phys. Rev. C* **70**, 024307 (2004).

[13] X. Viñas, M. Centelles, X. Roca-Maza, and M. Warda, *Density dependence of the symmetry energy from neutron skin thickness in finite nuclei*, *Eur. Phys. J. A* **50**, 27 (2014).

[14] T. Maruyama and T. Hatsuda, *Color molecular dynamics for high density matter*, *Phys. Rev. C* **61**, 062201(R) (2000) [nucl-th/9908021].

[15] Y. Akimura, T. Maruyama, N. Yoshinaga, and S. Chiba, *Molecular dynamics simulation for the baryon-quark phase transition at finite baryon density*, *Eur. Phys. J. A* **25**, 405-411 (2005).

[16] N. Yasutake and T. Maruyama, *Crossover equation of state based on color-molecular-dynamics*, *Phys. Rev. D* **109**, 043056 (2024) [nucl-th/2309.09632].

[17] N. Yasutake and T. Maruyama, *Equation of State Based on Color-Spin-Molecular Dynamics*, *Nucl. Phys. Rev.* **41**, QCS2023.06 (2024).

PoS(QCHSC24)221

[18] A. Park, S.-H. Lee, T. Inoue, and T. Hatsuda, *Baryon-baryon interactions at short distances: constituent quark model meets lattice QCD*, *Eur. Phys. J. A* **56**, 93 (2020).

[19] G. Baym, C. Pethick, and P. Sutherland, *The Ground State of Matter at High Densities: Equation of State and Stellar Models*, *Astrophys. J.* **170**, 299 (1971).

[20] A. Bauswein, O. Just, H.-T. Janka, and N. Stergioulas, *Neutron-star radius constraints from GW170817 and future detections*, *Astrophys. J. Lett.* **850**, L34 (2017) [astro-ph.HE/1710.06843].

[21] M. Shibata, E. Zhou, K. Kiuchi, and S. Fujibayashi, *Constraint on the maximum mass of neutron stars using GW170817 event*, *Phys. Rev. D* **100**, 023015 (2019) [astro-ph.HE/1905.03656].

[22] Y. Nara and H. Stoecker, *Sensitivity of the excitation functions of collective flow to relativistic scalar and vector meson interactions in the relativistic quantum molecular dynamics model RQMD.RMF*, *Phys. Rev. C* **100**, 054902 (2019).

PoS(QCHSC24)221